Biomedical Signal Processing and Control 75 (2022) 103560

Contents lists available at ScienceDirect

Biomedical Signal Processing and Control

journal homepage: www.elsevier.com/locate/bspc

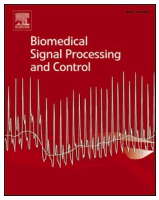

Automated cerebral microbleed detection using selective 3D gradient co-occurance matrix and convolutional neural network

Berakhah F. Stanley [a,*], S. Wilfred Franklin [b]

[a] Arunachala College of Engineering for Women, Tamil Nadu, India
[b] C.S.I Institute of Technology, Tamil Nadu, India

ARTICLE INFO

Keywords:
Cerebral Microbleeds
Co-occurance Matrices
MRI
Susceptibility Weighted Imaging
Convolutional Neural Network
Long Short Term Memory

ABSTRACT

Cerebral Microbleeds (CMBs) are small blood clots that form in the brains of many elderly and stroke victims. This promotes dementia as well as other physiological challenges in their daily activities. Early detection of CMBs is critical for limiting the long-term impacts that lead to confusing behavior. Because CMBs in the brain are so minute, manual identification by neurologists might be difficult at times, leading to misinterpretations. In this paper, we propound a newfangled feature extraction technique for the detection of CMB, by Selective 3D Gradient Co-occurance Matrix (S3DGCM). Our proposed framework efficiently detects the cerebral microbleeds (CMB) from magnetic resonance images by incorporating the Scharr Gradient operator with the concepts of the Co-occurance Matrix. The selected ROI was classified as CMB or non-CMB using a Convolutional Neural Network (CNN) classifier with Long Short Term Memory (LSTM) based on the extracted features from the S3DGCM. When compared with the previous methods, our method can extract more useful features which increase the accuracy rate in the detection process. The proposed work has been verified on two datasets containing MRI images with CMBs and Non-CMBs. The experimental results specify that our proposed scheme yields a promising result with the best sensitivity of 98.76%, specificity of 97.21%, an accuracy of 98.24%, and an F1-score of 98.76%.

1. Introduction

Cerebral Micro Bleeds (CMBs) are tiny, perivascular collections of brain parenchymal hemosiderins induced by the hemorrhages that occur in the human body. CMB's are hypointense lesions that may produce a larger endanger to future intracranial bleeds, cerebrovascular diseases such as cerebral angiopathy and it damages the cerebral small vessels. Due to the presence of CMBs, the zeal rate of ischemic stroke, Alzheimer's diseases, and traumatic brain injury are high. Studies show that 18% to 68% of the patients who are affected with ischemic stroke will have a ubiquity of CMBs [1]. CMBs are mainly caused by the emanation of the blood vessels. Rapid gradual cognitive decline, focal necrosis, convulsions, and headaches are the most common symptoms of CMBs. These are preponderant in the patients with stroke, dementia and sometimes identified in the healthier persons too [2]. Thus, in the recent years of remedial studies, the CMBs may have a genuine effect on neural function and traverse to a cognizable impairment such as dementia [3]. In this regard, it is relevant to detect the CMBs at the beginning. It is widely assumed that CMBs remain in the brain for several years. A large population-based study of over 800 people, with more than 200 participants presenting with cerebral microbleeds, discovered that just 6 people's CMBs vanished after 3.4 years of follow-up, while 85 other participants developed new CMBs. A subsequent study, however, contradicted this belief, demonstrating a decline in both the number and quantitative susceptibility.

As CMBs are hemosiderin occurred in the human, they can be detected with a magnetic field, since the hemosiderin is a strong paramagnetic material [4]. Therefore, it can be viewable in T2 Gradient Recalled Echo imaging (T2-GRE), Susceptibility Weighted Imaging (SWI), and 3D- T2 Gradient Recalled Echo imaging (T2-GRE) since these imaging schemes have an effect of ionization radiation [5]. The T2 weighted contrast is generated by using the gradient-echo (GRE) pulse sequence, where the echo time determines the amount of contrast. For 1.5 T, the echo time is 20–60 msec and 15–40 msec for 3.0 T in the case of T2 weighted imaging. In T2 weighted pulse sequences, the CMBs emerge as a small area of signal loss. But, in SWI Imaging, the CMBs are appeared to be in more contrast. SWI Imaging makes use of three-dimensional high-resolution completely flow-compensated GRE imaging with lengthy echo durations.

SWI is obtained from a high-resolution 3D gradient recalled echo

* Corresponding author.
E-mail address: berakhahs@gmail.com (B.F. Stanley).

https://doi.org/10.1016/j.bspc.2022.103560
Received 13 November 2021; Received in revised form 19 January 2022; Accepted 2 February 2022
Available online 12 February 2022

(GRE) scan in which the magnitude and phase images were saved. The phase images are subjected to a high pass (HP) filter to remove the unwanted artifacts. An enhanced contrast magnitude image is obtained by combining the magnitude image with the phase image and is known as the Susceptibility Weighted Imaging (SWI). In general, phase information makes it easier to distinguish CMBs from imitators like calcification. SWI Imaging allows for a more accurate depiction of CMBs when compared to the T2 weighted Imaging. According to the principle of magnetic susceptibility in brain tissue, MR imaging could help to distinguish between paramagnetic haemorrhages and diamagnetic calcifications. The paramagnetic blood products are extremely sensitive to SWI Imaging and therefore, the CMBs are visualized as small spherical zones with hypointensities. In SWI Imaging, the contrast-to-noise ratio of CMBs is greater. Furthermore, SWI is usually obtained at a higher spatial resolution than T2-GRE imaging. Several researchers have indicated that CMBs can be more visible on SWI than T2-GRE imaging. Therefore, Susceptibility Weighted Imaging (SWI) is used for the acquisition of CMBs.

Even though the CMBs are visualized in SWI more clearly than the T2-GRE imaging, the manual detection of CMBs will have errors, take more consumption of time, subjective with limited reproducibility, false diagnosis since the size of CMB is much small and it takes approximately 30 min to detect a CMB manually since its size varies from 2 mm to 10 mm. On the other hand, the automatic detection approaches can ease radiologist's burden while also improving the efficiency and reliability of radiologic evaluations. However, the automatic identification of CMBs is extremely problematic due to several challenges. They are (i) size from 2 mm to 10 mm (ii) the widely dispersed locations of CMBs make complete and precise detection even more difficult and (iii) there are numerous hard CMB mimics, such as flow holes, calcification, and cavernous malformations which resemble as such of CMBs. SWI Imaging makes these flow gaps, calcification, and cavernous malformations obvious. These factors decrease the ease of CMB detection from SWI-MRI Imaging.

This paper is arranged as follows: The related works are discussed in section 2. The proposed method is well described in section 3. The results and discussions are explained in section 4. Finally, the work is concluded in section 5 with its ideas for future enhancement.

2. Related works

Many investigations and methods were proposed in the last decennary for the computerized automatic identification of CMBs [6] since the manual detection was time consumable and error-prone. Some of the works incorporated handcraft methods and semi-automatic methods too. A semi-automatic method was proposed for the identification of CMBs based on thresholding mechanism and for classification Support Vector Machine (SVM) is used [7]. In this work, the true CMBs are identified based on the intensities within the image. Another semi-automated method is the 2D Fast Radial Symmetry Transform (2D-FRST) algorithm, which identifies the CMBs based on the minimum intensity values [8]. Another method used 7.0 T MR Images as input in which the 3D version of FRST was applied [9]. In this method, the 3D information of CMBs is extracted to detect the CMBs and obtain a sensitivity of 71.2%. But the false positives are removed manually. Random Forest model was developed which had obtained a sensitivity of 92% with 10.8 false positives per subject [10]. In recent years, Convolutional Neural networks are used in various applications such as cancer detection, tumor detection, and various medical applications [11] for the effective identifications of CMBs. In most of the works, CNN is used to reduce false positives [12].

Similarly, 3DGLCM is also widely used in medical imaging applications [13]. GLCM is used to extract the features in MRI Images and a fusion operator is used to increase the classification accuracy [14]. A two-stage approach was proposed for the automatic detection of CMBs from SWI Images [15]. This approach used FCN for screening the CMB areas and CNN for the discrimination stage. This approach has obtained average false positives per subject as 2.7, 44% as precision, and a sensitivity of 93.2%. 3D Residual Network was proposed for the detection of CMBs from phase images and SWI Images [16]. This scheme gives an average false positive per subject as 1.6, 70.9% as precision, and a sensitivity of 95.8%. The performance of detection is improved by using 2D FRST [17]. This resulted in average false positives per subject as 11.6, 72% as precision, and a sensitivity of 94.7%. A two-stage approach was proposed recently with a combination of YOLO and CNN for the automatic detection of CMBs [6]. This framework has obtained a precision of 61.9%, a sensitivity of 88.3%, and average false positives per subject of 1.4.

A combined probabilistic segmentation technique for detecting the CMBs from T2-Weighted MRI scan images [19] is proposed. This proposed technique has detected the CMBs in 8 from 13 patients more successfully but lost its capability when the subjects had a single CMB. A technique was introduced [20] based on the threshold values and 3D features are extracted from convolutional Independent Subspace Analysis (ISA) network which is an unsupervised algorithm followed by the classification phase that removes all the false positives. This technique brings out 89.44% of performance and false positives as 7.7. To detect the CMBs in the early stages, a new technique with the combination of Bayesian optimization and CNN was proposed [21]. To get a better performance the Bayesian optimization technique is used to find the optimal set of hyperparameters required for the machine learning algorithm. Five layers of CNN Network are used for the classification of the samples into CMBs and Non-CMBs. The main limitation of this work is that instead of feeding the first layer of CNN with 3D MR Images, it was fed with smaller slices of images. An undersampling technique is used for removing the imbalanced data between the Non-CMB voxel and the CMB voxels [22] and introduced a seven-layer Deep Neural Network (DNN). This DNN consists of the input layer, sparse autoencoder layer, softmax layer, and output layer and is introduced for the replacement of Convolutional Neural Network (CNN) since these techniques are very useful in deep learning methods. The autoencoder layer learns the features in an unsupervised learning method. The softmax classifier layer classifies the CMBs before the output layer based on the learning features obtained from the autoencoder layers, which are four in number. The limitation of this work is that the input SWI Images are obtained from different scanners that had different settings and contrast. Therefore, this method needs some image enhancement and compensation techniques.

Based on the deep learning approach, the CMBs are detected [23] using the combination of VGG, Extreme Learning Machine (ELM), and Gaussian Map Bat (GMB) algorithms. The VGG is a well-known Convolutional Neural Network (CNN) model, ELM is a learning algorithm that is used for training the feature vectors and GMB increases the efficiency of the ELM algorithm. The detection of CMBs is done with the help of stochastic pooling [24] and with the help of Convolutional Neural Network (CNN). Compared with the other pooling methods, the stochastic pooling method extracts more and more activation factor within the same region and uses the non-maximum activation factor. The CNN layer used in this work has 9 layers in which six layers are convolution layers and three layers are fully-connected layers. The limitation of this work is that the method is time-consuming.

In this paper, a new effective technique was proposed using SWI Images in which the true CMBs are detected even in the presence of ionization and calcification. The proposed method extracts the features based on the selective 3D gradient co-occurance matrices. In the classification stage, CNN is used which helps to discriminate the CMBs and Non-CMBs. LSTM network is used along with CNN structure, to retain the information from CNN, thus overcoming the problem of missed data in the object detection methods during the classification of CMBs. The objective of this paper is to accrete the accuracy and sensitivity in the detection of CMBs. The main contributions of our proposed work are as follows.

(i) Initially, the preprocessing of the input MRI Image is done using Gaussian filter and histogram equalization.
(ii) The Region of Interest (ROI) selection process is used to select the ROI from the preprocessed image.
(iii) A novel method Selective 3D Gradient Co-occurance Matrix (S3DGCM) is proposed, which is a feature extraction technique that extracts the features required for CMB classification. 3DGCM performs better in identifying the CMB even when the ROIs are non-monotonous.
(iv) The extracted features are given as a one-dimensional matrix to the CNN classifier for CMB/Non-CMB classification. The application of Long Short Term Memory (LSTM) along with CNN can make the proposed method generate an effective classification of CMBs and non-CMBs without human intervention.

3. Proposed method

The flow of the proposed framework is depicted in Fig. 1. The MRI input image is subjected to preprocessing before ROI selection and it is detailed in section 3.1. Followed by preprocessing is the ROI selection process which is explained in section 3.2. The features are extracted from the selected ROIs using the proposed 3DGCM, in which co-occurrence matrices are extracted from which the feature vectors were extracted, as explained in section 3.3. Lastly, in the final stage, a 1D CNN model is used to remove all false positives and to discriminate between CMBs and non-CMB images based on the feature vectors. A detailed description of the last stage can be found in Section 3.4.

3.1. Preprocessing of input image

Preprocessing is an initial stage in which the input image is changed

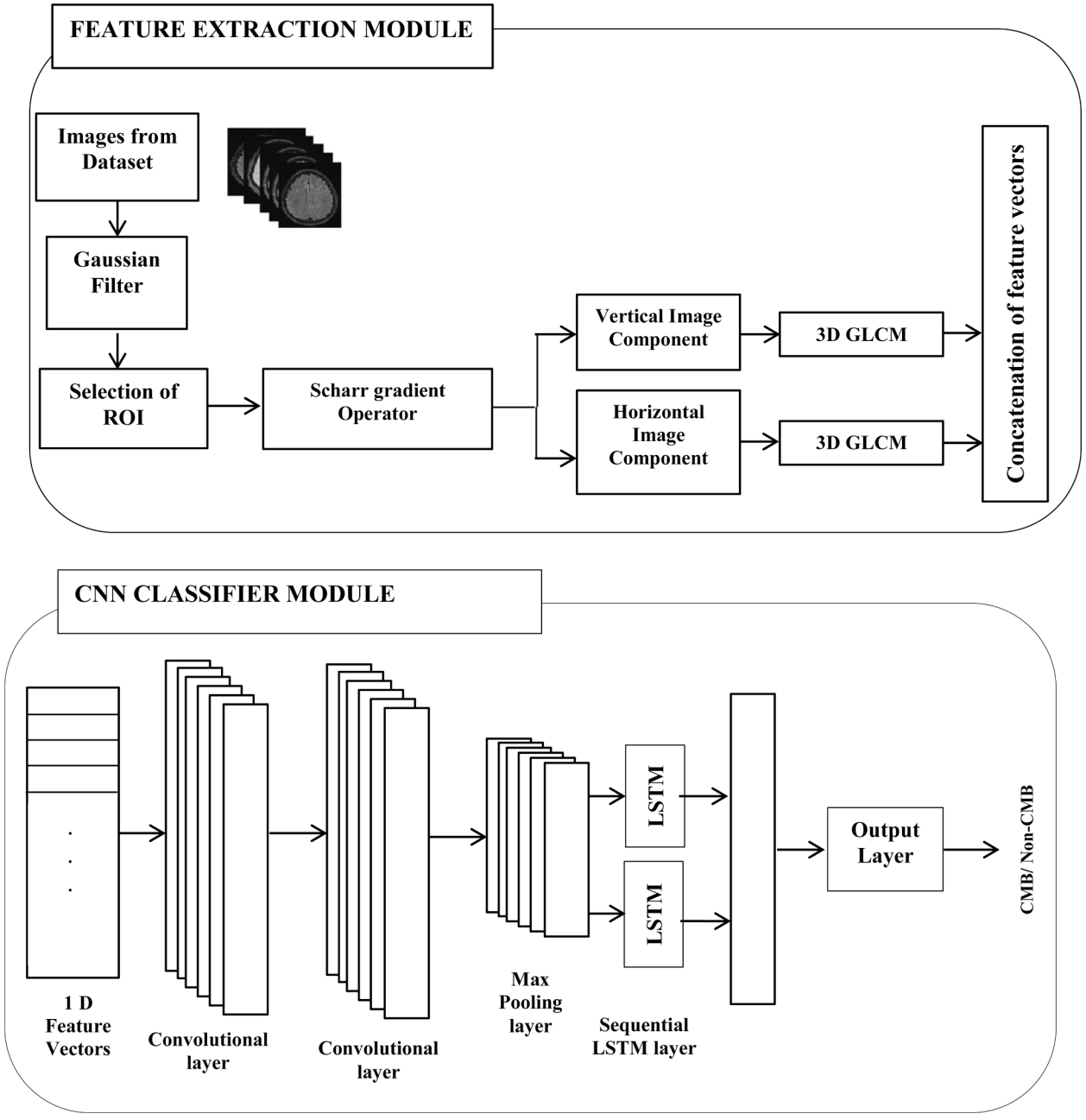

Fig. 1. Overall Block diagram of the proposed method.

to a format that is suitable for the next stages. Some of the commonly used MR Image preprocessing steps are image scaling, contrast stretching, normalization, etc. In this work, a Gaussian filter is applied to remove the noises present in the input image. The isotropic Gaussian has the form as given below:

$$G(x,y) = \frac{1}{2\pi\sigma^2} e^{\frac{-(x^2+y^2)}{2\sigma^2}} \quad (1)$$

where x represents the distance between the origin and the point in the horizontal axle, y represents the distance between the origin and the point in the vertical axle, and the standard deviation is represented by σ. The intensity of the entire image is normalized using the histogram equalization technique. It can be expressed as given below:

$$p_n = \frac{number\ of\ pixels\ with\ intensity\ n}{total\ number\ of\ pixels}, \quad n = 0, 1, 2, 3, ..., L-1, \quad (2)$$

The histogram equalized image g will be defined as given below:

$$g_{i,j} = floor((L-i)\sum_{n=0}^{k} p_n \quad (3)$$

where floor() represents the rounding off to the nearest integer. The preprocessing steps that are explained help us to design the automatic detection accurately.

3.2. Selection of ROI

This section explains the process of detecting the Region of Interest (ROI) from the filtered input image. The main goal of this task is to find the presumed area of CMBs. As an initial step, each greyscale color space of the filtered image is transformed into a binary image, thus the brain region can be crystalline. This binary image may consist of some noises and background information that could be removed by the morphological operation. The morphological operation comprises a set of the original image and structural element. The original image is the binary image and the structural element is a disk mask which is a matrix containing zeros and ones. Dilation and erosion are the two basic morphological operations. The dilation operation uses the structural element for probing and changes the image by growing in size ie; any background pixel connected to the object pixel will be replaced with the object pixel. These changes will be depending on the nature and shape of the structuring element. The erosion operation is the antipodal of dilation operation. It changes the image by dropping its size ie; any object pixel that touches the background pixel will be replaced with the background pixel. These changes will also depend on the nature and shape of the structuring element. The opening and closing operations are performed which is the mash-up operations of both dilation and erosion operation.

Once skull-free images are obtained after the morphological operations, ROI is identified based on the thresholding function. One of the important considerations that are done to identify the CMB area is its size. The size of the CMB defined in our work is from 7 to 35 number of pixels (2 mm to 10 mm). If the conditions are checked, the boundary box is created centered on the isolated candidate position which is the identified ROI. By the positions obtained from the boundary box (x coordinates and y coordinates), 3D block sizes are cropped from the original SWI MRI image. Thus, the skull stripped image is segmented effectively and on each of the cropped 3D block images, the feature extraction technique is applied to check the existence of CMBs.

3.3. Proposed feature extraction method

In this paper, a novel method is proposed for the extraction of the features which combines the Scharr gradient operator and 3D GLCM. The preprocessed cropped image is given to the Scharr gradient operator. This operator gives a greater accuracy when compared to the Sobel operators. Scharr gradient operator extracts three components namely the vertical, the depth, and the horizontal components. In this work, only the horizontal and the vertical components are considered for the further process since the depth component does not have much impact on CMB detection due to its small size. The horizontal and the vertical components are then subjected to 3D Gradient Co-occurance Matrix (3DGCM). To avoid the redundancy in 3DGCM, only selected GCM are considered for the extraction of features. A brief explanation of the feature extraction method is described as follows.

3.3.1. Calculation of 3D gradient image

The gradient is calculated using the ROI that was selected. Because the size of the CMB in our study is so small, the goal of finding the gradient is to discover it in such a way that the edges can be identified more accurately than other operators (2 mm to 10 mm). This gradient calculation aids in the highlighting of items in an image. Convolutional gradient operators are used in this work to boost the efficiency of identifying CMBs and thus, Scharr's Convolutional Gradient operators are employed here. A new technique was proposed to spot and highlight the gradient features for an image [25]. This gives better accuracy in the calculation of gradient derivatives and improved performance when compared with the existing filtering methods and is mainly used to recognize the changes in the pixel intensity.

When a gradient operator is applied to an image, it generates two responses vertical and horizontal. Although the vertical response is critical for distinguishing edge positions, the horizontal response is required for many operations that use edge orientation information, such as edge following, connecting, and grouping. Thus, we obtain 3D gradient vertical image (VI) and 3D gradient horizontal image (HI) from the selected ROI.

3.3.2. 3D gradient co occurance Matrix

The 3D gradient vertical and the horizontal images (VI and HI) that are extracted from the Scharr gradient operator are subjected to 3D GLCM to extract the feature vectors. Basically, in 2D the co-occurrence matrices are extracted by finding how often an intensity value occurs at the orientations 0°, 45°, 90° and 135° in distances of 1 and 2.

When expanding 2D GLCM to 3D GLCM, as like 4 orientations, a total of 13 orientations can be obtained as shown in Fig. 2. Let us consider either a vertical image (VI) or a horizontal image (HI), in which the

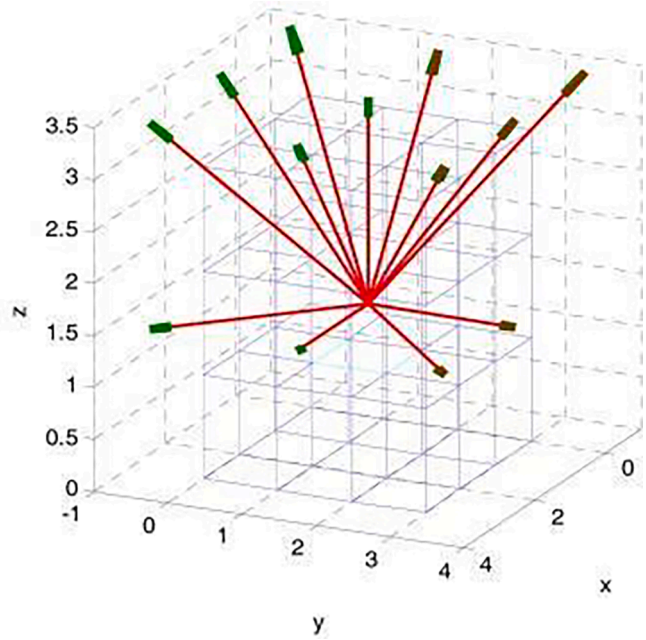

Fig. 2. Determination of 3D GLCM with distance d = 1 in 13 orientations.

number of times a grey level occurs is noted by the comparison with its neighbors or in the arbitrary region in VI or HI. Thus, the vertical image (VI) will have 13 3D Gradient co-occurrence matrices in the distance 1 (VI)1i, i = 1,2,3,…..,13 and 13 3D Gradient co-occurrence matrices in the distance 2 (VI)2i, i = 1,2,3,…..,13. Also, the horizontal image (HI) will have 13 3D Gradient co-occurrence matrices in the distance 1 (HI) 1j, j = 1,2,3,…..,13 and 13 3D Gradient co-occurrence matrices in the distance 2 (HI)2j, j = 1,2,3,…..,13. Thus, the neighbors are defined in 2 distances, and in total, VI, and HI in 3D GLCM results in 52 co occurance matrices.

3.3.3. Selection of 3D gradient co occurance matrix

The next step of the proposed system is to select the 3D gradient co occurance matrices from the 52 co occurance matrices based on some parameters. The computation of feature vectors from these 52 3D gradient co occurance matrices increases the complexity of the proposed work. [26] proposed a technique for the selection of feature vectors which was deliberately planned based on the weighted energy calculation and selecting only the maximum of it. The weighted energy value was determined from the normalization of energy I and normalization of energy II which is represented by the following expressions (4), (5), and (6).

$$Normalization\ Energy\ I(NormEI) = \frac{1}{M}\sum_{m=1}^{M}|I| \tag{4}$$

$$Normalization\ Energy\ II(NormEII) = \sqrt{\frac{1}{M}\sum_{m=1}^{M}|I|^2} \tag{5}$$

$$Weighted\ Energy\ Value\ (WEV) = \sqrt{(NormEI)^2 + (NormEII)^2} \tag{6}$$

The weighted energy value (WEV) of 52 3D gradient co occurance matrices is used in the selection procedure. The Weighted Energy Value (WEV) is generated for each 3D gradient co occurance matrix, yielding 52 WEV. The goal now is to choose a significant number of 3D gradient co occurance matrices for subsequent feature vector extraction. Now, let us consider the 26 3D gradient co occurance matrices from $(VI)_{1i}$ and $(HI)_{1j}$ with distance 1. Extracting the features from all the obtained 3D gradient co occurance matrices will lead to the possibility of redundant features which will increase the complexity of the system and degrade the detection accuracy. Hence, limited numbers of 3D gradient co occurance matrices are selected with the consideration of Weighted Energy Value (WEV) that is obtained by the equations (4), (5), and (6). The 3D gradient co occurance matrices are selected based on the calculated maximum weighted energy value with the grid search approach. The Selected 3D gradient co-occurance matrices by the above process are subjected to the further process for the extraction of features.

3.3.4. Estimation of features

The Selective 3D gradient co-occurance matrices that were chosen are now subjected to the feature extraction process. A count of 14 features is extracted as proposed in [27] and another 16 features are extracted from the extraction procedure proposed in [28]. The features that are extracted are angular second-moment contrast, correlation, variance, inverse difference moment, sum average, sum variance, sum entropy, entropy, difference variance, difference entropy, information measures of correlation I, information measures of correlation II, maximal correlation coefficient, maximum probability, median probability, first quartile probability, third quartile probability, deviation of probability, autocorrelation, cluster average, cluster variance, cluster shade, cluster prominence, dissimilarity, inverse difference, homogeneity II, information measures of correlation III, information measures of correlation IV and difference average. As a result, 30 features are extracted from each 3D gradient co occurance matrix, yielding feature vectors that are concatenated in a one-dimensional matrix.

Algorithm of the proposed Feature Extraction Methodology

Input: Training Image, $[I_{train}]$
Output: Set of features, $[F_{image}]$
1) Preprocess the input image by applying the Gaussian filter by using equation (1).
2) Apply histogram equalization by using the equations (2) and (3).
3) ROI selection
   (i) Calculation of binary image.
   (ii) Apply the morphological operations.
   (iii) Identify the ROIs by thresholding mechanism.
4) Apply the Scharr gradient operator to calculate the 3D Gradient Horizontal Image (HI) and 3D Gradient Vertical Image (VI) from the selected ROI obtained from step (3).
5) Calculate the 3D GLCM for VI to obtain the 3D Gradient Co occurance Matrices in distance 1 $((VI)_{1i})$, i = 1,2,3,4,….,13 and distance 2 $((VI)_{2i})$, i = 1,2,3,4,….,13. This results in 26 3D Gradient Co occurance Matrices.
6) Similarly, calculate the 3D GLCM for VI as like step (5) to obtain $((HI)_{1j})$, j = 1,2,3,4,….,13 in distance 1 and $((HI)_{2j})$, j = 1,2,3,4,….,13 in distance 2. Thus, results in 26 3D Gradient Co occurance Matrices.
7) Compute the Weighted Energy Value (WEV) for the obtained 3D Gradient Co occurance Matrices from steps (5) and (6) using the eqns (4), (5), and (6).
8) Select the 3D Gradient Co occurance Matrices that have the maximum value of WEV in distance 1. $(MD1)_n = \max\{(VI)_{1i}, (HI)_{1j}\}$, i,j = 1,2,3,4,….,13. Where, n = 1,2,….,15.
9) Similarly, select the 3D Gradient Co occurance Matrices in distance 2. $(MD2)_n = \max\{(VI)_{2i}, (HI)_{2j}\}$, i,j = 1,2,3,4,….,13. Where, n = 1,2,…,18.
10) Extract the feature vectors from the Selective 3D Gradient Co occurance Matrices obtained from steps (8) and (9). The number of features extracted is 30 from one Selective 3D Gradient Co occurance Matrix.
11) After extracting the entire feature vectors from 33 Selective 3D Gradient Co occurance Matrices, the features are kept in a one-dimensional array.
12) This one-dimensional array is given to the CNN classifier module for the detection of CMBs.

3.4. 1D-CNN classifier module

1D Convolutional Neural Networks (1D CNNs) is a modified variant of 2D CNNs which have recently been developed. Researchers have proven that 1D CNNs are superior to their 2D counterparts in dealing with 1D vectors for certain applications. The sole difference between 1D and 2D CNN is that the inputs, kernels, and feature mapping are indeed one-dimensional. There are two layers in 1D CNN, namely, (i) Convolution and max-pooling layer and (ii) Fully connected layer. There are two convolution layers, a max-pooling layer and a layer of fully connected neurons. In our methodology, the CNN classifier module consists of three layers, namely (i) Convolution and Max pooling layer, (ii) Long Short Term Memory (LSTM) layer, and (iii) Fully Connected Layer.

As in 2D CNN, 1D CNN has the input as 1D feature vectors and the output will depend on the number of classes. In our methodology, the input was the one-dimensional feature vectors and the output classes were two in number, namely, the CMB and non-CMB. Initially, the convolution layers are provided with 1-dimensional input feature vectors, which map the features by convolving the input image with the kernel. The max-pooling layer captures more information and decreases dimension. In the realm of deep learning, Long Short Term Memory (LSTM) is a valuable architecture for automatic detection. Long-term dependencies are common in deep learning processes and may be overlooked during processing. To eliminate long-term dependency, LSTM is employed, which employs memory cells [29,30]. Each LSTM layer is made up of a cell, an input gate, an output gate, and a forget gate. The cell remembers the time interval, and the gates are responsible for information flow within the cell. The fully connected layers employ the softmax activation function to obtain probabilities of the input belonging to a specific class.

4. Results and discussion

4.1. Dataset

The first dataset (SWI-CMB Dataset) contains SWI images from 320

subjects that are captured from the 3.0 T Philips Medical System in which the settings are done: repetition time is 17 ms, volume size is 512x512x150, echo time is 24 ms, 2 mm slice thickness with the resolution of 0.45x0.45 mm^2 and field of view is 230x230 mm^2 [15]. The dataset has been checked by expert radiologists.

The second dataset (SVS-CMB Dataset) contains SWI images captured from 179 subjects acquired by Siemens 3.0 T Verio and Skyra MRI scanners with the following parameters: repetition time of 27 ms and 40 ms, echo time of 20 ms and 14 ms, flip angle (FA) of 15°, pixel bandwidth (BW) of 120 Hz/pixel and slice thickness of 2 mm [6]. The description of the two datasets is represented in Table 1.

Fig. 3 depicts some of the SWI MRI images included in the dataset, which are labeled with CMBs. There is more than one CMB in a brain image in some of the scans.

4.2. Experimentation

Experiments are carried out on the SWI-CMB and SVS-CMB datasets. The SWI-CMB dataset contains 924 CMB Images acquired from 320 subjects and SVS-CMB Dataset contains 572 CMB Images from 107 subjects, as shown in Table 1. The first step in our methodology is preprocessing after which the identification of ROI was done by the involvement of skull stripping and morphological operations. To identify the ROIs effectively, the thresholding method is used since the size of the CMBs is very small (2 mm-10 mm). The value of the threshold is chosen as 70 (pixel value) since the sensitivity of the proposed work is high when it is 70 and is tabulated in Fig. 4. The requirement for ROI arises from the fact that the entire image may contain calcifications and other structures larger than 10 mm or smaller than 2 mm in size. Only the structures with dimensions ranging from 2 mm to 10 mm are required to be identified as CMBs. As a result, the size of structures above and below this range is excluded from the analysis. Since the involvements of all the ROIs make our proposed system complex. As a result, we meticulously extract the ROIs from each image in the datasets using bounding boxes.

The performance of the proposed technique is measured by five parameters namely, the sensitivity, specificity, False Positive Rate, accuracy, and F1 score which are represented as follows:

$$\text{Sensitivity} = \frac{True\ Positive}{True\ Positive + False\ Negative} \tag{7}$$

$$\text{Specificity} = \frac{True\ Negative}{True\ Negative + False\ Positive} \tag{8}$$

$$\text{False Positive Rate} = \frac{False\ Positive}{True\ Negative + False\ Positive} \tag{9}$$

$$\text{Accuracy} = \frac{True\ Positive + True\ Negative}{True\ Positive + True\ Negative + False\ Positive + False\ Negative} \tag{10}$$

$$\text{F1 score} = \frac{2 \times True\ Positive}{2 \times True\ Positive + False\ Negative + False\ positive} \tag{11}$$

The proposed method in this analysis uses p fold cross-validation (p = 10) to improve the effectiveness and reliability of the proposed framework. For this, the CMB and the Non-CMB images in each of the datasets are divided into 10 subsets randomly and are mentioned in Table 1. Out of the 10 subsets, 9 subsets are utilized for training and the remaining subset is utilized for testing. This process is repeated again and again with the other subsets too. In each of the p folds, the true positives, true negatives, false positives, and false negatives are measured to verify the correctness of the proposed method. From these values, the parameters in equations (7), (8), (9), (10), and (11) are evaluated. After the 10 folds, in the SWI-CMB Dataset, we obtain an average sensitivity of 98.76%, average specificity of 97.21%, average false positive rate of 3.46, an average accuracy of 98.24, and an average F1 score of 98.76%. For SVS-CMB Dataset, the obtained values of average sensitivity, average specificity, average false positive rate, average accuracy, and average F1- score are 98.07%, 97.36%, 2.59, 97.83%, and 98.31% respectively. The obtained values for the SWI-CMB dataset and SVS-CMB dataset are displayed in Table 2.

Table 1
Dataset Overview.

Dataset	SWI-CMB Dataset	Training	Testing	SVS-CMB Dataset	Training	Testing
Subjects	320	230	90	179	107	72
CMBs	1149	924	225	760	572	188

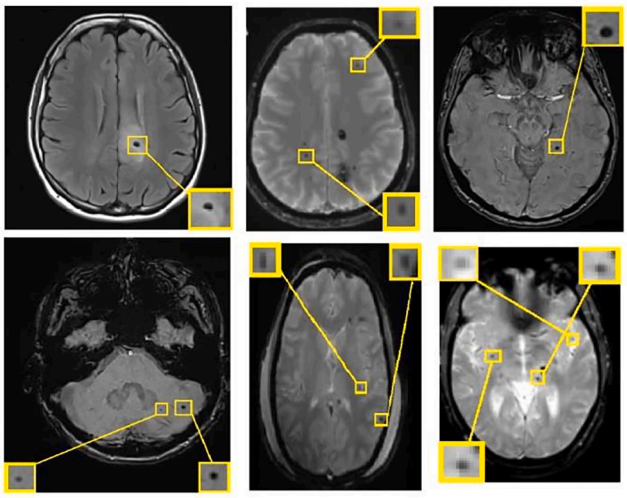

Fig. 3. Sample Images from the SWI-CMB Dataset with CMBs marked in it.

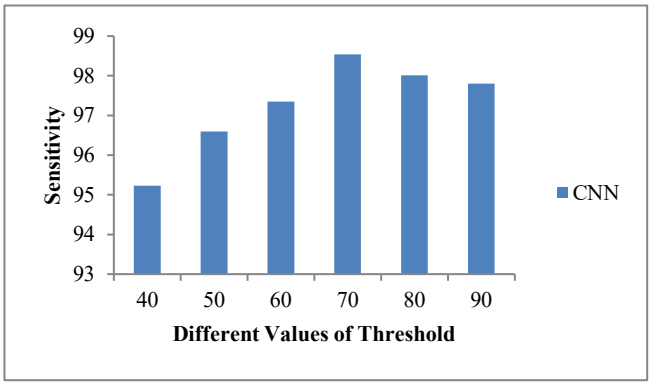

Fig. 4. Sensitivity rate of CNN classifier on various values of threshold.

Table 3 denotes the selection of the 3DGCMs based on the maximum weighted energy value (WEV) on the co occurance matrices. There is a need of selecting the 3DGCMs to reduce the complexity of the proposed framework. Therefore, we use the grid search approach for the selection of 3DGCMs from each of the datasets. After this approach, we obtain the Selective 3D Gradient Co occurance Matrices (S3GCM). From Table 3, it can be noted that SWI-CMB Dataset gives its maximum accuracy when the selected number of Selective 3D Gradient Co occurance Matrices is 15 at distance 1 (MD1 = 15) and 18 at distance 2 (MD2 = 18). Similarly, for SVS-CMB Dataset the maximum accuracy is obtained when the selected number of Selective 3D Gradient Co occurance Matrices is 17 at distance 1(MD1 = 15) and 18 at distance 2 (MD2 = 18).

In the ROI detection process, the input SWI MRI Image is subjected to an enhancement process and then it is converted to binary.

Table 2
Performance of the proposed feature extraction technique in the 10-fold Cross-Validation procedure for the SWI-CMB Dataset and SVS-CMB Dataset.

Test set	SWI-CMB Dataset					SVS-CMB Dataset				
	Sensitivity	Specificity	False Positive Rate	Accuracy	F1-score	Sensitivity	Specificity	False Positive Rate	Accuracy	F1-score
Fold 1	99.31	97.5	2.5	98.9	99.3	98.48	96.77	3.2	97.94	98.48
Fold 2	98.65	97.2	2.7	98.37	98.98	96.83	97.06	2.9	96.91	97.6
Fold 3	96.7	97	2.9	96.7	98	98.36	94.44	5.5	96.91	97.56
Fold 4	99.28	97.83	2.1	98.9	98.2	98.51	96.67	3.3	97.94	98.51
Fold 5	99.3	95.12	4.8	98.37	99	98.34	97.14	2.8	97.9	98.39
Fold 6	99.3	97	3	99	99.3	96.77	97.14	2.8	96.91	97.56
Fold 7	98.7	97	3.3	98.3	99	98.36	97.22	2.7	97.94	98.36
Fold 8	98.52	97.44	8.8	96.7	97.8	96.72	97.22	2.7	96.9	97.5
Fold 9	98.6	98	2.3	98.3	98.9	100	100	0	100	100
Fold 10	99.28	98	2.2	98.9	99.2	98.39	100	0	98.97	99.19
Average fold	**98.76**	**97.21**	**3.46**	**98.24**	**98.76**	**98.07**	**97.36**	**2.59**	**97.83**	**98.31**

Table 3
Selection of number of 3DGCMs based on the accuracy value for the SWI-CMB Dataset and SVS-CMB Dataset.

MD1	MD2	SWI-CMB Dataset	SVS-CMB Dataset
1	5	92.32	93.6
3	10	92.95	93.9
6	9	94.35	94
10	4	97.21	93.54
13	15	98	94.8
15	**18**	**98.24**	95.23
17	**18**	97.9	**97.83**
20	22	97.58	96.22
23	25	97.11	97.44
26	26	96.85	97.0

Morphological operations are performed to reduce noise and to generate a skull-free image. After which a bounding box is created over each of the CMB regions with the consideration of thresholding (pixel value > 70) and size (7 to 35 number of pixels). This bounding box has a size in 3D since the SWI MRI image is 3D in nature. Hence, 3D blocks are cropped from the original SWI MRI Image by the same position of the created bounding box. The size of these blocks was carefully chosen for effective validation. Initially, a block size of 14x14x12 is chosen and by enlarging the block size, more additional contextual information can be obtained to better distinguish CMBs from their mimics. As the size of the 3D block size gets altered, the value of the evaluation parameter gets changed as depicted in Table 4. In our work, we choose the input block size as 20x20x16, because the sensitivity, precision, and average false positives are comparatively higher when compared to the other block size configurations. We try the varied configurations of 3D block size to validate more information and to increase the detection rate. The values of the evaluation parameters are tabulated in Table 4.

Receiver Operating Characteristics (ROC) for the different configuration of 3D block sizes is depicted in Fig. 5. When the 3D block size is14x14x12, the sensitivity of the proposed work is 97.31%, the specificity value is 96.5% and the average false positive rate is 4.2. These values are improved when the block size is changed to the size 18x18x12. Now, the sensitivity becomes 98.02%, specificity becomes 97% and the average false positive gets reduced to 4. When the 3D block size is 20x20x16, the sensitivity obtained is 98.76%, the specificity obtained is 97.21% and the average false positive rate becomes 3.46. This gives an optimal detection performance when compared with the other

Table 4
Result of detection process based on different configurations of Block sizes.

3D Block Size	Sensitivity	Specificity	Average False Positives
14×14×12	97.31%	96.5%	4.2
18×18×12	98.02%	97%	4
20×20×16	**98.76%**	**97.21%**	**3.46**
24×24×20	97.56%	96.5%	5.2

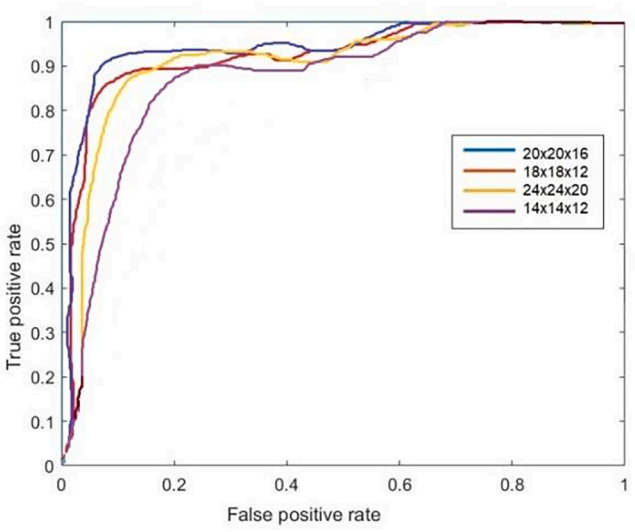

Fig. 5. ROC Curve for the different 3D block size configuration.

3D block sizes.

As the 3D block size is changed to 24x24x20, the detection sensitivity becomes 97.56%, specificity becomes 96.5% and the average false positive rate is 5.2. Thus, in our experiment, the 3D block size of 20x20x16 was chosen since it provides a higher sensitivity value due to the Scharr gradient values in vertical and horizontal directions when compared to the other configurations.

ROC shown in Fig. 6 was based on the different models used in the field of detecting the CMBs from SWI MRI Images as shown in Table 5. In the below table, at first, we use our proposed method S3DGCM with the SVM method. Here SVM is mainly used to extract the features. When using such a combination, we obtain less sensitivity 90.58%, specificity as 89.12%, and average false positive as 7.2. When using CNN, we obtain a sensitivity of 95.32%, specificity of 93.57%, and an average false positive rate of 5.1. The last model is the proposed method, in which we obtain 98.76% sensitivity, 97.21% specificity, and 3.46 average false positive rate. From Table 5 and Fig. 6, we can conclude that our method outperforms the other two models in terms of sensitivity, specificity, and average false positive rate.

This comparison shows that the proposed technique outperforms the

Table 5
Detection Results for Various models.

Methods	Sensitivity	Specificity	Average False Positives
S3DGCM + SVM	90.58%	89.12%	7.2
CNN	95.32%	93.57%	5.1
S3DGCM + CNN	**98.76%**	**97.21%**	**3.46**

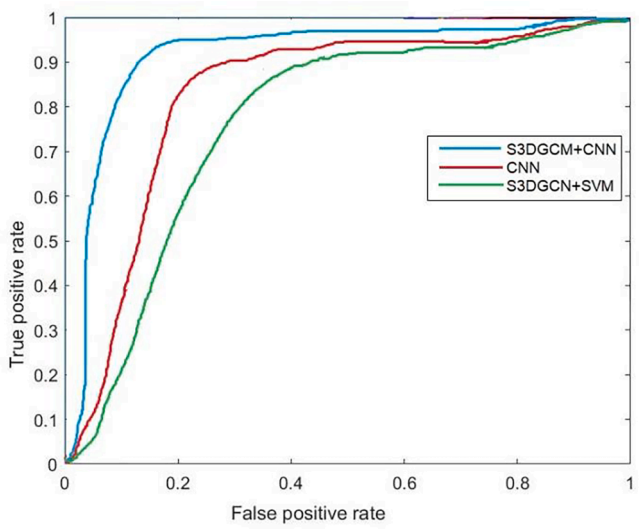

Fig. 6. ROC Curve for Different Methods.

other two methods in terms of detection sensitivity and average false-positive rates. As a result, when compared to CNN's performance, our proposed technique provides superior information. As a result, utilizing CNN during the classification stage increases the method's accuracy and performance.

The comparison chart is obtained and is tabulated in Table 6. The comparison is made between our proposed feature extraction method with the conventional SVM method, CNN, and at last by the combination of the proposed framework with CNN on different datasets. The SWI-CMB Dataset in Table 6 denotes that for the accuracy calculation, the training and testing images are taken from the same dataset. Similarly, for SVS-CMB Dataset, the training and testing images are taken from the same SVS-CMB dataset. In the cross dataset, the training set is initially the complete SWI-CMB Dataset, and the testing set is initially the entire SVS-CMB Dataset and vice versa. When using our proposed method along with the Support Vector Machine gives an accuracy of 90.58%, 95.32%, and 98.76% for SWI-CMB Dataset, SVS-CMB Dataset, and cross Dataset respectively. By using the Convolutional Neural Network, we get an accuracy of 95.12% for SWI-CMB Dataset, 96.57% for SVS-CMB Dataset, and 94.21% for cross datasets. When using our proposed method with the combination of CNN gives an accuracy rate of 98.2%, 97.87%, and 95.78% for SWI-CMB Dataset, SVS-CMB Dataset, and cross Dataset respectively. This shows that the performance of our proposed method is better compared with the other methods. Our proposed method shows better performance due to the gradient values generated through the Scharr operators and the application of the 3DGLCM technique that shows a better performance in the field of object recognition.

4.3. Discussion

In recent years, many examinations and exertions have been carried out for the automatic detection of CMBs from MRI images. The main challenges of automatic detection are widespread of CMBs in the brain image, the small size of CMB which is 2 mm to 4 mm and the presence of CMB mimics that is ionizations and calcifications in the brain surface. Using SWI Image in the field of automatic detection is needed since; these SWI Images are enormously delicate to the local tissue susceptibility and the paramagnetic blood surfaces. There is a need for automatic detection since manual identification is extremely untruthful due to the presence of CMB mimics and is time-consuming. In this regard, we propose a novel technique which is a combination of Selective 3D Gradient Co occurance Matrix (S3DGCM) and Convolutional Neural Network (CNN). At first, the input SWI MRI Image is subjected to pre-processing since the naturally acquired Image will have noises even it is 3D in nature and this may degrade detection accuracy. Therefore, Gaussian filters are used for noise removal. Then, the histogram equalization is done to increase the reliability of our proposed work.

Table 6
Accuracy rate for various methods.

Methods	S3GDCM + SVM	CNN	S3GDCM + CNN
SWI-CMB Dataset	90.58%	95.12%	**98.24%**
SVS-CMB Dataset	92.32%	96.57%	**97.83%**
Cross Dataset	89.76%	94.21%	**95.78%**

The image is next subjected to ROI detection because we only need lesions that are between the stated size ranges of 2 mm-10 mm. This is accomplished by the use of a threshold value, after which the bounding box on each of the lesions is fixed. This method is more practical in that it allows new radiologists to easily identify lesions, reducing time consumption. This promotes the radiologists to inspect the patient more carefully. After the ROI detection, the ROI is subjected to the Scharr Gradient operator, this generates the vertical and horizontal gradient Images. These gradient operators help to enhance the edges, easy to detect the edges and orientations. Each of the gradient operators is applied with 3D GLCM, which is very advantageous that this technique is well suited for object detection applications. From this, 3DGLCM is applied in distance = 1,2 thus we get Co occurance matrices. The features are extracted from the selected co occurance matrices, to decrease the complexity of our proposed work. In the classifier module, 1D CNN is used. Most of the previous approaches use 2D CNN for processing the 3D datas [18], but in our proposed method we use 1D CNN for classification, recently, some works used 3D CNN on medical images [15]. By applying the 1D CNN, we can able to detect the CMBs more clearly with more effortful output.

For analysis, we have considered two sets of datasets SWI-CMB Dataset and SVS-CMB Dataset that are from the existing works [15,6]. In each of the datasets based on folding operation, the training and testing are done within the dataset and across the datasets. When compared with the other conventional methods, the CNN along with our proposed work gives better performance due to the calculation of gradient images and the extraction of features from 3D GLCM.

A table of comparison is presented in Table 7 that comprises a detailed report on the parameters of the technique that is proposed and the existing methods on the detection of CMBs. The main crucial challenge is the separation of the true cerebral microbleeds in the presence of calcifications for the correct diagnosis and accordingly providing suitable treatment. In the current scenario, the generation of Susceptibility Weighted Imaging (SWI) is the essential source for the sharpened visualization of cerebral veins without the lack of enhancing it. The reason is that the susceptibility of the local tissue and microbleeds are very much sensitive only in SWI Images.

As shown in Table 7, most of the existing works use the fast radial symmetry transform (FRST) as a detection method [8–10]. The first one that is discussed in Table 7 gives a sensitivity of 50% and the detection time/ subject is less than 3 min [32]. The statistical thresholding algorithm is used in the second work gives an increased sensitivity of 81.7% when compared with the first method. This method used handcrafted features based on the intensity and shape [7]. 2D Radial Symmetry Transform is used in [8], which produces a sensitivity of 86.5%. The FRST is one of the methods that use the local radial symmetry to trace out the spherical regions present in the brain images. It is noted that the proposed method outperforms the most commonly applied FRST method on the detection of the CMBs and achieves high sensitivity and a minimum average false positive rate. Here, 3D-FRST is implemented to check the ability to detect the CMB potential candidates against the proposed work [10]. The 3D-FRST worked with the sensitivity of 92.04%, but at the same time generated more number of average false positive rate. The 3D-FRST method which is used generates very high bulky training samples even after intensifying the CMB samples; this

Table 7
Performance comparison of the proposed method with the existing methods.

Reference	Method	Performance	
		Sensitivity	Time/ subject
Seghier et al. [32]	MIDAS	50%	<3 min
Barnes et al [7]	Statistical Thresholding Algorithm	81.7%	–
Bian et al [8]	2D Radial Symmetry Transform	86.0.5%	1 min
Fazlollahi et al [10]	Radon based features + Radom Forest Classifier	92.04%	–
Kuijf et al [9]	3D Radial Symmetry Transform	71.20%	1.5 min
Dou et al [20]	3D hierarchical features and Independent Subspace Analysis (ISA) network	89.44%	40 sec
Van Den Heuvel et al [31]	Computer Aided Detection (CAD)	90%	–
Dou et al [15]	3D Convolutional Neural Network (CNN)	93.2%	64 sec
Liu et al [16]	3D-ResNet	95.8%	29 sec
Chen et al [17]	3D-ResNet	94.69%	–
Wang et al [33]	2D-DenseNet	97.78%	–
Hong et al [34]	2D-ResNet-50	95.71%	–
Mohammed et al [6]	YOLO and 3D-CNN	94.32%	33 sec
Zhang et al [22]	Seven-layer Deep Neural Network (DNN)	95.13%	–
Lu et al [23]	VGG and ELM trained by Gaussian Map Algorithm	93.08%	–
Wang et al [24]	Nine layer CNN with stochastic pooling	97.22%	–
Proposed Work	**Selective 3D Gradient Co occurance Matrix (S3DGCM) + CNN**	**98.76%**	**15 sec**

may affect the overall performance.

3D Radial Symmetry Transform is used in [9], it obtained a less sensitivity of 71.20%. 3D hierarchical features and Independent Subspace Analysis (ISA) network is used in [20], it does not use any deep learning processes it gives an average sensitivity of 89.44%. The result of 3D-CNN also shows that it does not affect the average false positive rate, but it gives a reduced sensitivity when compared to our proposed work.

High performance in terms of sensitivity and precision can be noticed and achieved in [17,16,33,34] is due to the very huge number of CMB images taken for the experiment compared to the other studies. The number of images used [16] is 1641 CMB images from 220 subjects, [17] extracted 2835 CMB images from 73 subjects, Wang S H et al. [33] experimented with 68,847 CMB images from 20 patients and the number of images selected for experimentation in [34] is 4287 CMBs from 10 subjects. The running time per subject for the proposed method and state-of-art methods are depicted in Table 7. Our method gives better performance in time complexity when compared with other methods. This is because the S3DGCM method adapted here performs the linear operation and hence, the time complexity needed is O(mxnxz), where, mxnxz represents the 3D image size. The time complexity for the 1D CNN utilized here is O(n.k.d), where, n is the length of the input, k is the dot products and d is the multiplications performed. Due to the less time complexity of our proposed method, compared with the other methods, the running time per subject is less. Our proposed work requires 15 s for one subject, which is 4 times faster than the 3D CNN method Dou et al [15].

The proposed method gives an effective and feasible performance with very good experimental results. This is because of the feature extraction algorithm that is used which extracts all the gradient values which makes the edges sharp and the application of S3DGCM gives a better performance in identifying small-sized lesions. The benefits of our proposed work require less computation time, works well even when the data are less and it can detect multiple CMBs from an image.

5. Conclusion

Identifying CMBs in the human brain is critical for aged people since it leads to greater difficulties in their bodies. Patients with Cerebral Microbleeds go undiscovered for a long time, and if they have a severe or critical COVID-19 infection, the untreated CMB leads to a grave state [35]. As a result, radiologists and clinicians must notice the existence of CMBs to properly diagnose patients and exercise necessary caution when prognosticating patients. When the detecting process is done by hand, it is an extremely arduous and time-consuming task. With the help of 1D CNN, we have implemented an effective and new approach for automated detection. The 3D GLCM used in this study efficiently retrieves CMB lesions from SWI MRI images. The CNN eliminates the greatest number of false positives, resulting in high sensitivity, specificity, accuracy, and a lower average false positive rate.

Funding

The authors received no specific funding for this work.

Declaration of Competing Interest

The authors declare that they have no known competing financial interests or personal relationships that could have appeared to influence the work reported in this paper.

References

[1] A. Charidimou, P. Kakar, Z. Fox, D.J. Werring, Cerebral microbleeds and recurrent stroke risk: systematic review and meta-analysis of prospective ischemic stroke and transient ischemic attack cohorts, Stroke 44 (4) (2013) 995–1001.
[2] S. Martinez-Ramirez, S.M. Greenberg, A. Viswanathan, Viswanathan, A Cerebral microbleeds: overview and implications in cognitive impairment, Alzheim. Res. Therapy 6 (3) (2014) 33, https://doi.org/10.1186/alzrt263.
[3] A. Charidimou, A. Krishnan, D.J. Werring, H. Rolf Jäger, Cerebral microbleeds: a guide to detection and clinical relevance in different disease settings, Neuroradiology 55 (6) (2013) 655–674.
[4] T.P.L. Roberts, D. Mikulis, Neuro MR: principles, J. Magn. Reson. Imaging 26 (4) (2007) 823–837, https://doi.org/10.1002/jmri.21029.
[5] W. Chen, W. Zhu, I. Kovanlikaya, A. Kovanlikaya, T. Liu, S. Wang, C. Salustri, Y. i. Wang, Intracranial calcifications and hemorrhages: characterization with quantitative susceptibility mapping, Radiology 270 (2) (2014) 496–505.
[6] M.A. Al-masni, W.-R. Kim, E.Y. Kim, Y. Noh, D.-H. Kim, Automated detection of cerebral microbleeds in MR images: a two-stage deep learning approach, NeuroImage: Clin. 28 (2020) 102464, https://doi.org/10.1016/j.nicl.2020.102464.
[7] S.R.S. Barnes, E.M. Haacke, M. Ayaz, A.S. Boikov, W. Kirsch, D. Kido, Semiautomated detection of cerebral microbleeds in magnetic resonance images, Magnetic Resonance Imaging 29 (6) (2011) 844–852, https://doi.org/10.1016/j.mri.2011.02.028.
[8] W. Bian, C.P. Hess, S.M. Chang, S.J. Nelson, J.M. Lupo, Computer-aided detection of radiation-induced cerebral microbleeds on susceptibility-weighted MR images, NeuroImage: Clin. 2 (2013) 282–290, https://doi.org/10.1016/j.nicl.2013.01.012.
[9] H.J. Kuijf, J. de Bresser, M.I. Geerlings, M.M.A. Conijn, M.A. Viergever, G. J. Biessels, K.L. Vincken, Efficient detection of cerebral microbleeds on 7.0 T MR images using the radial symmetry transform, NeuroImage 59 (3) (2012) 2266–2273, https://doi.org/10.1016/j.neuroimage.2011.09.061.
[10] A. Fazlollahi, F. Meriaudeau, V.L. Villemagne, C. Rowe, P. Yates, O. Salvado, P.T. Bourgeat, Efficient machine learning framework for computer-aided detection of cerebral microbleeds using the radon transform, in Proceedings of the IEEE-ISBI conference, 2014.
[11] M.A. Al-masni, M.A. Al-antari, J.-M. Park, G. Gi, T.-Y. Kim, P. Rivera, E. Valarezo, M.-T. Choi, S.-M. Han, T.-S. Kim, Simultaneous detection and classification of breast masses in digital mammograms via a deep learning YOLO-based CAD system, Comput. Methods Programs Biomed. 157 (2018) 85–94.
[12] H. Chen, L. Yu, Q. Dou, L. Shi, V.C. Mok, P.A. Heng, Automatic detection of cerebral microbleeds via deep learning based 3d feature representation. Proceedings of the IEEE-ISBI Conference, 2015.
[13] A. Depeursinge, A. Foncubierta-Rodriguez, D. Van De Ville, H. Müller, Three-dimensional solid texture analysis in biomedical imaging: Review and opportunities, Med. Image Anal. 18 (1) (2014) 176–196.
[14] M. Khalil, H. Ayad, A. Adib, Performance evaluation of feature extraction techniques in MR-Brain image classification system, Procedia Comput. Sci. 127 (2018) 218–225.
[15] Q. Dou, H. Chen, L.Q. Yu, L. Zhao, J. Qin, D.F. Wang, V.C.T. Mok, L. Shi, P.A. Heng, Automatic Detection of Cerebral Microbleeds From MR Images via 3D

Convolutional Neural Networks, IEEE Transactions on Medical Imaging, pp.1182–1195,2016. doi: 10.1109/TMI.2016.2528129.
[16] S. Liu, D. Utriainen, C. Chai, Y. Chen, L. Wang, S.K. Sethi, S. Xia, E.M. Haacke, Cerebral microbleed detection using Susceptibility Weighted Imaging and deep learning, Neuroimage 198 (2019) 271–282.
[17] Y. Chen, J.E. Villanueva-Meyer, M.A. Morrison, J.M. Lupo, Toward automatic detection of radiation-induced cerebral microbleeds using a 3D deep residual network, J. Digit. Imaging 32 (5) (2019) 766–772.
[18] H. R. Roth, L. Lu, J. Liu, J. Yao, A. Seff, C. Kevin, L. Kim, and R. M. Summers, "Improving computer-aided detection using convolutional neural networks and random view aggregation," arXiv preprintar Xiv:1505.03046, 2015.
[19] S. Sangiem, K. Dittakan, K. Temkiavises, S. Yaisoongnern, Cerebral Mirobleed Detection by Extracting Area and Number from Susceptibility Weighted Imagery Using Convolutional Neural Network Journal of Physics: Conference Series 1229 012038, 2019. doi: 10.1088/1742-6596/1229/1/012038.
[20] Q. Dou, H. Chen, L. Yu, L. Shi, D. Wang, V.C. Mok, Heng PA Automatic cerebral microbleeds detection from MR images via independent subspace analysis based hierarchical features, in: 37th annual international conference of the IEEE engineering in medicine and biology society (EMBC), 2015, pp. 7933–7936.
[21] P. Doke, D. Shrivastava, C. Pan, Q. Zhou, Y.-D. Zhang, Using CNN with Bayesian optimization to identify cerebral micro-bleeds, Machine Vision and Applications 31 (5) (2020), https://doi.org/10.1007/s00138-020-01087-0.
[22] Y.-D. Zhang, Y. Zhang, X.-X. Hou, H. Chen, S.-H. Wang, Seven-layer deep neural network based on sparse autoencoder for voxelwise detection of cerebral microbleed, Multimedia Tools and Applications 77 (9) (2018) 10521–10538, https://doi.org/10.1007/s11042-017-4554-8.
[23] S. Lu, K. Xia, S. Wang, Diagnosis of cerebral microbleed via VGG and extreme learning machine trained by Gaussian map bat algorithm, J. Ambient Intelligence Humanized Comput. (2020), https://doi.org/10.1007/s12652-020-01789-3.
[24] S. Wang, J. Sun, I. Mehmood, C. Pan, Y.i. Chen, Y.-D. Zhang, Cerebral micro-bleeding identification based on a nine-layer convolutional neural network with stochastic pooling, Concurrency and Computation: Practice and Experience 32 (2019), https://doi.org/10.1002/cpe.5130.
[25] H Scharr, Optimal operators in digital image processing. PhD thesis (2000).
[26] R. Jeen Retna Kumar, M. Sundaram, N. Arumugam, V. Kavitha, Face feature extraction for emotion recognition using statistical parameters from subband selective multilevel stationary biorthogonal wavelet transform, Soft Comput. 25 (7) (2021) 5483–5501, https://doi.org/10.1007/s00500-020-05550-y.
[27] R.M. Haralick, K. Shanmugam, I. Dinstein, Textural features for image classification, IEEE Trans. Systems Man and Cybernetics 3 (6) (1973) 610–621.
[28] Y. Hu, Z. Liang, B. Song, H. Han, P.J. Pickhardt, W. Zhu, C. Duan, H. Zhang, M. A. Barish, C.E. Lascarides, Texture feature extraction and analysis for polyp differentiation via computed tomography colonography, IEEE Trans. Med. Imaging 35 (6) (2016) 1522–1531, https://doi.org/10.1109/TMI.2016.2518958.
[29] F. Chollet, Deep Learning with Python, 1st ed., Manning Publication Co., Greewich, CT, USA, 2017.
[30] I. Goodfellow, Y. Bengio, A. Courville, Deep Learning, MIT press (2016).
[31] T. Van den Heuvel, M. Ghafoorian, A. van der Eerden, B. Goraj, T. Andriessen, B. ter Haar Romeny, B. Platel, Computer aided detection of brain micro-bleeds in traumatic brain injury, in SPIE Medical Imaging International Society for Optics and Photonics, pp. 94142F–94142F, 2015. doi: 10.1117/12.2075353.
[32] M.L. Seghier, M.A. Kolanko, A.P. Leff, H.R. Jäger, S.M. Gregoire, D.J. Werring, Microbleed detection using automated segmentation (MIDAS): a new method applicable to standard clinical MR images, PloS One 6 (3) (2011) e17547.
[33] S. Wang, C. Tang, J. Sun, Y. Zhang, Cerebral micro-bleeding detection based on densely connected neural network, Front. Neurosci. 13 (2019), https://doi.org/10.3389/fnins.2019.00422.
[34] J. Hong, H. Cheng, Y.D. Zhang, J. Liu, Detecting cerebral microbleeds with transfer learning, Machine Vision and Applications, pp.1123–1133, 2019.
[35] N.A. Gupta, C. Lien, M. Iv, Critical illness-associated cerebral microbleeds in severe COVID-19 infection, Clin. Imaging 68 (2020) 239–241.